AD-A083 340 SCIENCE APPLICATIONS INC LA JOLLA CA F/G 18/3
A HIGH ALTITUDE IONIZATION STRUCTURE AND SCINTILLATION MODEL.(U)
FEB 79 D L SACHS DNA001-78-C-0196
UNCLASSIFIED SAI-023-79-562-LJ DNA-4828F NL

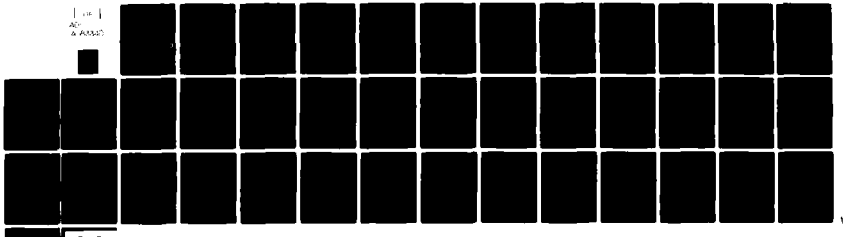

END
DATE FILMED
5-80
DTIC

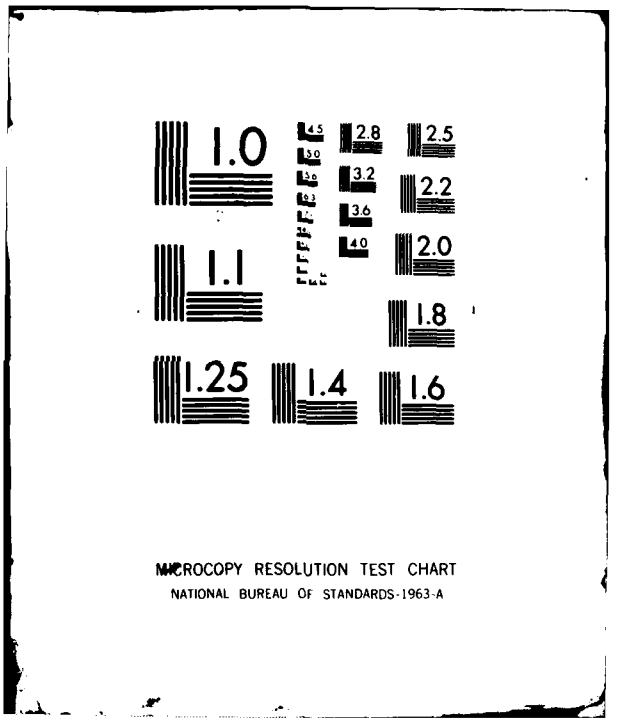
1.0
1.1
1.25
1.4
1.6
1.8
2.0
2.2
2.5
2.8
3.2
3.6
4.0
4.5
5.0
5.6
6.3
7.1
MICROCOPY RESOLUTION TEST CHART
NATIONAL BUREAU OF STANDARDS-1963-A

(1) LEVEL III

AD-E 300 711

DNA 4828F

# A HIGH ALTITUDE IONIZATION STRUCTURE AND SCINTILLATION MODEL

Science Applications, Inc.
1200 Prospect Street
La Jolla, California 92038

19 February 1979

Final Report for Period 1 May 1978—31 January 1979

CONTRACT No. DNA 001-78-C-0196

APPROVED FOR PUBLIC RELEASE;
DISTRIBUTION UNLIMITED.

DTIC
ELECTE
APR 24 1980
S D
B

THIS WORK SPONSORED BY THE DEFENSE NUCLEAR AGENCY
UNDER RDT&E RMSS CODE B322078464 S99QAXHB05417 H2590D.

Prepared for
Director
DEFENSE NUCLEAR AGENCY
Washington, D. C. 20305



80 3 20 069

Destroy this report when it is no longer needed. Do not return to sender.

PLEASE NOTIFY THE DEFENSE NUCLEAR AGENCY, ATTN: STTI, WASHINGTON, D.C. 20305, IF YOUR ADDRESS IS INCORRECT, IF YOU WISH TO BE DELETED FROM THE DISTRIBUTION LIST, OR IF THE ADDRESSEE IS NO LONGER EMPLOYED BY YOUR ORGANIZATION.

UNCLASSIFIED

SECURITY CLASSIFICATION OF THIS PAGE *(When Data Entered)*

| REPORT DOCUMENTATION PAGE | | READ INSTRUCTIONS BEFORE COMPLETING FORM |
|---|---|---|
| 1. REPORT NUMBER<br>DNA 4828F | 2. GOVT ACCESSION NO.<br>AD-A083 340 | 3. RECIPIENT'S CATALOG NUMBER |
| 4. TITLE *(and Subtitle)*<br>A HIGH ALTITUDE IONIZATION STRUCTURE AND SCINTILLATION MODEL | | 5. TYPE OF REPORT & PERIOD COVERED<br>Final Report for Period<br>1 May 78—31 Jan 79 |
| | | 6. PERFORMING ORG. REPORT NUMBER<br>SAI-023-79-562-LJ |
| 7. AUTHOR(s)<br>David L. Sachs | | 8. CONTRACT OR GRANT NUMBER(s)<br>DNA 001-78-C-0196 |
| 9. PERFORMING ORGANIZATION NAME AND ADDRESS<br>Science Applications, Inc.<br>1200 Prospect Street<br>La Jolla, California 92038 | | 10. PROGRAM ELEMENT, PROJECT, TASK AREA & WORK UNIT NUMBERS<br>Subtask S99QAXHB054-17 |
| 11. CONTROLLING OFFICE NAME AND ADDRESS<br>Director<br>Defense Nuclear Agency<br>Washington, D.C. 20305 | | 12. REPORT DATE<br>19 February 1979 |
| | | 13. NUMBER OF PAGES<br>42 |
| 14. MONITORING AGENCY NAME & ADDRESS*(if different from Controlling Office)* | | 15. SECURITY CLASS *(of this report)*<br>UNCLASSIFIED |
| | | 15a. DECLASSIFICATION/DOWNGRADING SCHEDULE |

16. DISTRIBUTION STATEMENT *(of this Report)*

Approved for Public Release; distribution unlimited.

17. DISTRIBUTION STATEMENT *(of the abstract entered in Block 20, if different from Report)*

18. SUPPLEMENTARY NOTES

This work sponsored by the Defense Nuclear Agency under RDT&E RMSS Code B322078464 S99QAXHB05417 H2590D.

19. KEY WORDS *(Continue on reverse side if necessary and identify by block number)*

Scintillation
Satellite Link
Striations
Nuclear Effects Code

20. ABSTRACT *(Continue on reverse side if necessary and identify by block number)*

A method is described for the implementation of a time dependent striation structure and convection model into an existing systems code. The purpose is to update estimates of the scintillation effects of the structuring of the ionization of high altitude nuclear bursts on satellite radio signals.

The structure and convection model is an extrapolation of the results of a numerical calculation for an idealized situation to the nuclear case combined with a late time bifurcation model.

DD FORM 1 JAN 73 1473 EDITION OF 1 NOV 65 IS OBSOLETE

UNCLASSIFIED

SECURITY CLASSIFICATION OF THIS PAGE *(When Data Entered)*

## TABLE OF CONTENTS


| Section | | Page |
|---|---|---|
| | LIST OF ILLUSTRATIONS . . . . . | 2 |
| 1 | INTRODUCTION . . . . . | 3 |
| 2 | THE STRUCTURE MODEL . . . . . | 7 |
| 3 | IMPLEMENTATION OF STRUCTURE AND CONVECTION INTO FIREBALL MODEL . . . . | 21 |
| 4 | SCINTILLATION EFFECTS . . . . . | 32 |
| 5 | IMPLEMENTATION INTO AN EXISTING CODE . | 36 |
| 6 | LIST OF REFERENCES . . . . . | 38 |

## LIST OF ILLUSTRATIONS


| Figure | | Page |
|---|---|---|
| 1 | Initial Contours NRL 3716 . . . . . | 8 |
| 2 | Final Contours NRL 3716 . . . . . | 10 |
| 3 | Intermediate Contours NRL 3716 . . . . . | 15 |
| 4 | Later Contours NRL 3864 . . . . . | 17 |
| 5 | Contours in Plane of Magnetic Field . . . . . | 22 |
| 6 | Contours in Plane Perpendicular to Field . . . . | 23 |

# 1. INTRODUCTION AND SUMMARY

This report describes how to implement into an existing satellite lines status computer code, the author's current state of understanding of the structuring and convection of ionization from a high-altitude-nuclear-explosion and the resultant scintillation of radio signals penetrating the structure. The existing code must be or use RANC IV Mod 3, a nuclear effects code built by G. E. Tempo for the D. N. A. [1]

The changes are simple and straightforward and can easily be implemented in other codes which use the RANC phenomenology routines.

These codes currently use a description of ionization structure obtained from the radiance profile of a single late time nuclear burst. This structure is time-independent and has a power spectrum that decreases exponentially in wave-number. It is currently believed that the power spectrum of the ionization of typical bursts will have a power law form which leads to greater scintillation effects at SHF and above than would be due to an exponential form. [2]

It must be stressed that the changes that we are making in the structure description are not the result of a complete and consistent treatment of the physics of the structuring process. That treatment has not yet been done by anyone in the community of contractors to the DNA. What has been done by this community is a numerical nonlinear analysis of the structuring of ionization with a one-dimensional Gaussian variation in the direction of a constant neutral wind. [3,4]

We explain in Section 2 how the results of this numerical analysis lead to insights into the structuring to be expected in the ionization of a late-time nuclear burst.

From these insights we suggest a model of the time dependent structuring of the ionization which specifies parameters of the structure that relate directly to scintillation descriptions. These parameters do not uniquely follow from the

numerical analysis. There may be alternate models and parameters that are a better representation of the structure. We view the modeling described herein as a first cut to demonstrate the feasibility of the concept of this type of approach to the fast-running scintillation model and invite other members of the community of contractors to devote some of their time to its improvement.

When structuring begins, the ionization is able to convect across magnetic field lines. Current codes do not include this effect but restrain the ionization by magnetic containment. We use the results of the same numerical analysis to model this convection.

In Section 3 we describe how we implement the structure and convection model into the RANC fireball model using the results of a hydro code calculation[5] to guide the correspondence between the numerical analysis results and the nuclear case. In Section 4 we describe the scintillation effects in terms of the parameters of structure and ionization content using extensions of results obtained in a previous study.[6]

In Section 5 we describe the suggested method of implementing the structure and scintillation model into the existing code. A by-product is a change in the calculated absorption to be consistent with the changed ionization model.

The essential concepts of the stucture and convection model are: There is a period of time after a high altitude burst when expansion across the ambient magnetic field has ceased and the ionization is constrained by the magnetic field. We use the time TEQ from the RANC code for this period.

After this time neutrals continues to have a radial component of velocity across the magnetic field causing the gradient drift instability to be operative. The results of a numerical calculation of the effects of that instability on the structuring and convection of a one-dimensionally varying plasma is applicable for scaling the initial structuring and convection of the nuclear plasma. The motion of the plasma in the direction of the magnetic field and the time variation of the electron density are uncoupled from the structuring and convection across the field and are taken from the RANC code. There is a scaled time after TEQ when structuring has begun internally but the radius to the boundary of the

ionization as given by RANC, RTF, has not changed. After this time the boundary radius grows with time at a constant rate as large fingers of ionization protrude radially whose tips bifurcate into smaller fingers of lesser electron density until all the ionization is in the two sets of fingers. After this time the ionization in the large fingers flows into the smaller fingers which have bifurcated again. Finally, the small fingers continuously bifurcate until a minimum size is reached.

## 2. THE STRUCTURE MODEL

The structure model is based on the following concepts. First, the various two-fluid hydrocodes (e.g., MELT, built by MRC) are useful for the prediction of the early time (< 500 sec.) distribution of ionization following a high-altitude nuclear burst and the conditions which cause structuring (neutral wind, gravity, etc.). They cannot, however, describe the structuring that does occur because of the very large (~ 100 km) cell size they must use. After structuring should have occurred, these codes will be incorrect not only by the absence of the structuring but also by the absence of the convection of the ionization across magnetic field lines because of the structuring.

Second, an illustration of the structuring and convection unobtainable from the hydrocodes is given by the output of a numerical electrostatic code such as one existing at NRL.

The only example of such a calculation that we feel is pertinent to this nuclear structuring problem was done for the case of a plasma in a uniform magnetic field.[3,4] The plasma had a Gaussian variation of density in one direction superimposed on a constant background. The problem was done for the case of a uniform electric field at right angles to the magnetic field and to the density gradient. This is completely equivalent to the case of a uniform neutral wind blowing through the plasma at right angles to the electric and magnetic fields in the gradient direction. In the absence of perturbations the plasma would remain stationary with the drag of the neutral wind balanced by a magnetic force ($\vec{J} \times \vec{B}$). The situation at the beginning of the calculation is illustrated in Figure 1 taken from the NRL report.[3] The neutral wind is in the y direction and the current that balances the drag is in the x direction and varies only with y.

The pertinence of this calculation to the nuclear case is the high ratio of the maximum density to the background and the lack of variation of the plasma in the direction of $\vec{J}$. In the nuclear case the plasma geometry is essentially cylindrical with the axis along a relatively uniform magnetic field. The density

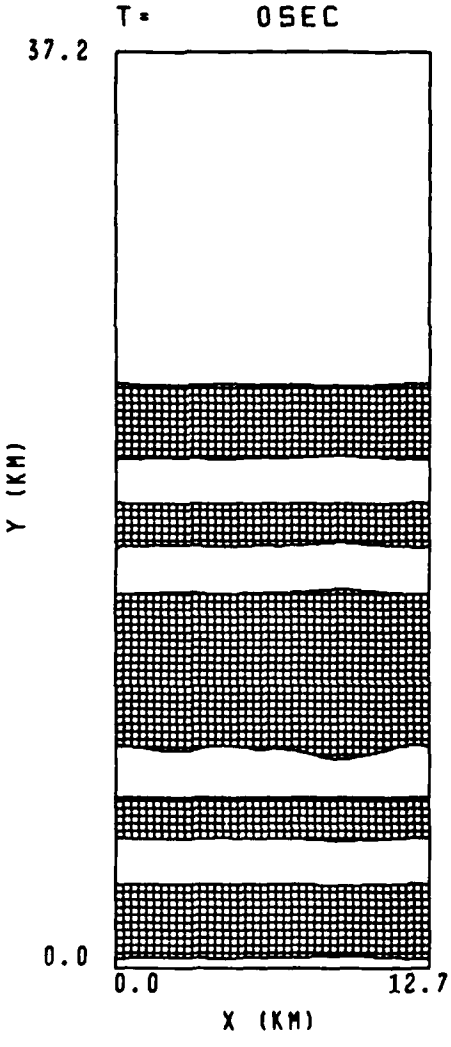


Fig. 16. Isodensity contours of plasma density at $t = 0$ sec. The initial destribution for $N_e/N_o$ is a gaussian in $y$, centered at $y = 12.1$ km, plus a small random perturbation in $x$. Contours are drawn for $N_e/N_o = 1.5$, 3.5, 5.5, 7.5 and 9.5. The area between every other contour line is cross-hatched. Only 120 of the 160 cells actually used in the $y$ direction are displayed. Boundary conditions are periodic in both directions. In our plot $\mathbf{B}_o$ is toward the reader, and $\mathbf{E}_o$ is directed toward the right, and we have placed outselves in a frame moving with the $(c/|B_o|^2)\,\mathbf{E}_o \times \mathbf{B}_o$ velocity. The upper portion of the gaussian is physically unstable to perturbations, while the lower half is (linearly) stable.

**Figure 1. Initial Contours NRL 3716.**

variation and the neutral wind direction is radial. The current is azimuthal and varies in the radial direction. The structuring begins near the edge of the plasma where a cartesian approximation to radial-azimuthal variation is best. The subsequent behavior of the edge of the plasma in response to the small perturbations in the numerical calculation is similar to the behavior expected at the edge of the nuclear plasma during the first phase of its structuring. This is illustrated in Figure 2 taken from the same report. These figures indicate certain concepts of structure that are useful for the modeling philosophy.

Before describing these concepts we will review the insights obtained from analysis of the simple problem of an elliptic cylindrical plasma cloud of constant conductivity $\Sigma_c$, with axis along a constant magnetic field $\vec{B} = B\hat{z}$, imbedded in a background plasma of conductivity $\Sigma_b$. A neutral wind of uniform velocity $\vec{V} = V\hat{y}$ blows through the plasma. If the background plasma is not moving in the region far from the cloud, there is no electric field in that region. The cloud boundary contains a polarization surface charge producing an electric field in and near the cloud. The motion of the cloud or background plasma is governed by the equation

$$\vec{V}_p = \frac{\vec{E} \times \vec{B}}{B^2} .$$

The electric field is found from the equations

$$\vec{\nabla} \cdot \vec{J} = \vec{\nabla} \times \vec{E} = 0$$

$$\vec{J} = \Sigma(\vec{E} + \vec{V} \times \vec{B}) = \Sigma(\vec{E} + VB\hat{x}) .$$

where far from the cloud, $\vec{J}_\infty = \Sigma_b VB\hat{x}$. There is a discontinuity in the normal component of $\vec{E}$ at the cloud boundary because of the discontinuity in $\Sigma$. From the divergence theorem $\vec{J}_c \cdot \hat{n} = \vec{J}_b \cdot \hat{n}$ or $\Sigma_c(\vec{E}_c + VB\hat{x}) \cdot \hat{n} = \Sigma_b(\vec{E}_b + VB\hat{x}) \cdot \hat{n}$, where $\hat{n}$ is a unit normal at the boundary. Adding and subtracting $\Sigma_c \vec{E}_b \cdot \hat{n}$ obtains the formula for the surface charge

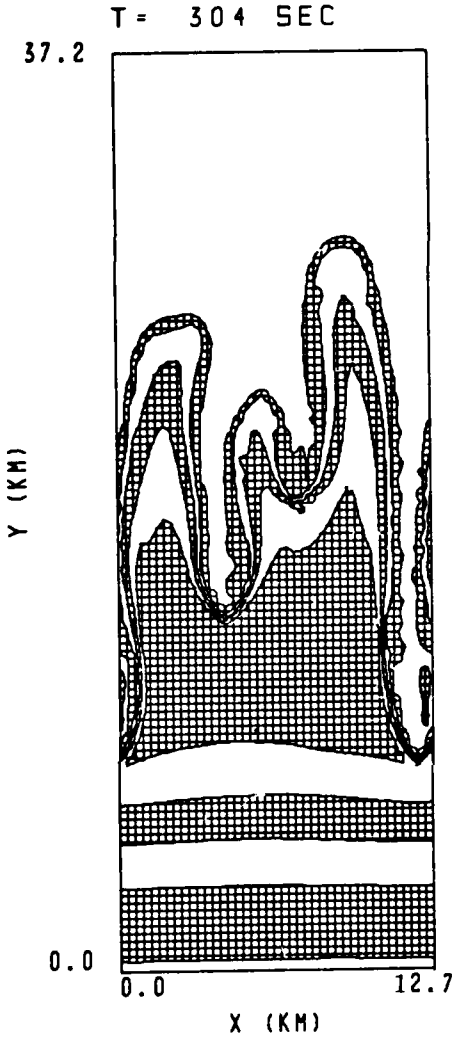


Fig. 19. Same as Fig. 16, but for $t$ = 304 sec. Development is fully nonlinear, as the intense gradients and associated high Fourier wave numbers become apparent.

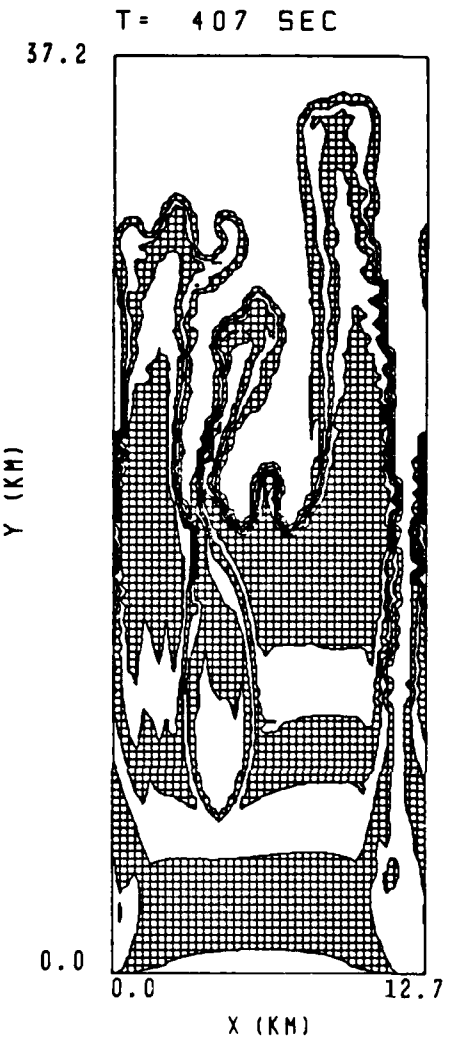


Fig. 20. Same as Fig. 16, but for $t$ = 407 sec. Several plasma bifurcations are apparent, in agreement with the experimental results from ionospheric barium cloud releases, and we have maximum to minimum density variations resolved over only 2 cells.

Figure 2. Final Contours NRL 3716.

$$\sigma \equiv (\vec{E}_b - \vec{E}_c) \cdot \hat{n} = \frac{(\Sigma_c - \Sigma_b)}{\Sigma_c \Sigma_b} \vec{J} \cdot \hat{n} \qquad (1)$$

choosing $\hat{n}$ to point to the background.

The solution for the electric field everywhere is obtained by the usual procedure for a dielectric in a field which is uniform at infinity. Set $E = -\nabla\varphi$ where $\nabla^2\varphi = 0$ within and without the plasma cloud and $\varphi \to 0$ at infinity. At the boundary, $\varphi$ is continuous and $\nabla\varphi$ has a jump according to the surface charge density $\sigma$.

For the special case of an elliptic cloud with ratio of y intercept to x intercept $\beta$, an analytic solution shows that the electric field within the cloud is uniform with value

$$\vec{E}_c = -VB\hat{x} \frac{\left(1 - \frac{\Sigma_b}{\Sigma_c}\right)}{\left(1 + \frac{\Sigma_b}{\beta\Sigma_c}\right)} .$$

The cloud moves as a whole with velocity $\vec{E}_c \times \vec{B}/B^2$. For the usual case where $\beta\Sigma_c >> \Sigma_b$, the velocity is $\vec{V}_c \approx V\hat{y}(1 - \Sigma_b/\Sigma_c)$. At the boundary $\vec{E}_b \cdot \hat{n} = -(1/\beta)\vec{E}_c \cdot \hat{n}$ and the interior current

$$\vec{J} = \frac{\vec{J}_\infty(1 + \beta)}{(\Sigma_b/\Sigma_c + \beta)} \approx \vec{J}_\infty \left(1 + \frac{1}{\beta}\right) .$$

The insights gained from the elliptical problem are

- The higher the conductivity ratio, the more the cloud moves with the neutral wind.
- The higher the elongation in the wind direction the less the exterior electric field and change in current.
- If $\beta >> 1$ and $\Sigma_b > \Sigma_c$, the cloud moves against the neutral wind with a speed greater than neutral wind speed by a

$$\text{factor} \left\{ \beta/[1 + \beta(\Sigma_c/\Sigma_b)] \right\}.$$

We use these insights to describe some of the qualitative behavior shown by the conductivity contours in Figure 2. The initial configuration was

$$\Sigma = 1 + 10e^{-(y/8)^2} [1 + \epsilon(x, y)]$$

where $\epsilon$ was generated from a $K^{-4}$ power spectrum with random phases and $\epsilon_{rms} = 0.03$. There is a neutral wind of 100 m/s in the y direction. The contours are $\Sigma = 1.5,\ 3.5,\ 5.5,\ 7.5,\ 9.5$.

From the two figures it is apparent that

- Fingers of high conductivity move slower than fingers of low conductivity that go against the wind. The plasma therefore separates into many large blobs in a short time.
- The steepening occurs at the lower conductivity contours in the plasma fingers. This is because the change in electric field and hence the change in velocity is proportional to $\sigma$ which by expression (1) is proportional to $(\Sigma_c - \Sigma_b)/\Sigma_c$ since J is relatively uniform. The Gaussian profile in y becomes broader until $\Sigma \sim 5.5$ where it steepens abruptly. The x profile of course is the finger width.
- Two backgroundfingers descended with little resistance. The high conductivity interior and the lower region of decreasing conductivity do not begin to move until the fingers pass them. Because of the periodic boundary conditions, the voltage drop across the mesh remains zero, i.e., $\varphi(x = 0) = \varphi(x = L)$. Therefore the lower regions do not experience an electric field until the passage of the low conducitivity finger with its own electric field requires an exterior electric field to keep

$$\int_0^L E_x dx = 0 \ .$$

The behavior of the third background finger in the central region is different since it is not in a uniform background of high conductivity. Its bifurcation produced a steep small high conductivity finger. It is interesting that the other plasma fingers appear to have median values of $\Sigma$ where they tend to form necks prior to break off. This signifies small striations with low values of central conductivity occurring in many cases with the bulk of the peak values of conductivity in the central region of large striations.

By about 450 sec., the NRL run ends showing two main highly elongated fingers of width 3 km and two smaller fingers of smaller length and width, one high density and one at lower average density. The trifurcation that appears in the one finger in the figure also begins in the other main figure at 450 sec. We do not understand the tendency to trifuracate in the NRL calculation. We can speculate that the tendency of the finger to flatten and steepen sets the stage for the next phase of fingering and in the case of the NRL calculation, a 0.3 km cell size and a 3 km finger width limits the number of new fingers to three. The tendency to flatten and steepen is apparent in Figure 2. The finger on the right has moved an average velocity of 60 m/s between the two times whereas the $\Sigma = 5.5$ and 7.5 contours have moved an average of 80 m/s. The finger on the left undergoing trifurcation has moved at 50 m/s. The boundary of the plasma has moved 12 km during the calculation time for an average initial convection speed during the first phase of 30 m/s.

We must now scale the results of the NRL calculation to what we expect to occur in the first phase of structuring in the ionization from a high altitude nuclear burst. The first question we address is the size of the fingers to be expected. The NRL run had fingers of width 3 km. Although the Gaussian scale length for the radial $\Sigma$ dependence was 8 km, the arguments put forth in Chapter 4 of a previous analysis,[6] indicate the real scale length in question is the minimum value of

$$h \equiv |\nabla \ell n \Sigma|^{-1}$$

which is 4.7 km for the NRL case. A 3 km finger corresponds to a wavelength of 6 km so that defining $k = 2\pi/\lambda$, we have $kh_{min} \approx 5$ which we take as the scaling

required to estimate finger width in the nuclear case.

The next question we address is the scaled time required to finish the first phase of fingering which was about 450 sec. in the NRL case. According to the linear instability theory, the growth rate = $1/\tau_g \approx V/h_{min}$ or $\tau_g = 47$ sec. Since they started with 3% perturbations, the nonlinear phase should begin at $t = \tau_g \ln 33 = 3.5\,\tau_g = 165$ sec. This occurs in the narrow region of maximum growth (minimum h) illustrated in Figure 3. It takes a little longer for the last contour ($\Sigma = 1.5$) to resemble the contour of the budding fingers. We take as the time for the background to have fingered in sufficiently to begin rapid movement through the cloud as $4\,\tau_g$. Now the problem should begin to resemble the previously described analytic case of an ellipse in a constant background except the background is not constant. In that case an ellipse made up of background conductivity flowing through a constant cloud of higher conductivity went against the neutral wind with a speed

$$V_b \approx \frac{V\left(\frac{\Sigma_c}{\Sigma_b} - 1\right)}{1 + \frac{\Sigma_c}{\beta\Sigma_b}} > V \ .$$

The nonuniformity of the background should reduce this speed by an unknown amount. Referring back to Figure 2 we see qualitative agreement in that background fingers go faster than plasma fingers but the two background fingers seem to be travelling at ~90 m/s between 300 and 400 sec. Comparison of Figures 2 and 3 show the speeds to be 90 and 135 m/s between 200 and 300 sec. Thus the nonuniformity of the background reduces the analytic speed expected considerably.

Since the NRL calculation with its constraint that the polarization electric field average to zero over the x dimension of the mesh should be more similar to the nuclear case (where the azimuthal electric field should have zero average) than the analytic case of uniform infinite bakcground, we choose our scaling of the background finger speed from the NRL case. We take the background finger speed as the neutral wind speed. Thus the time for this phase will

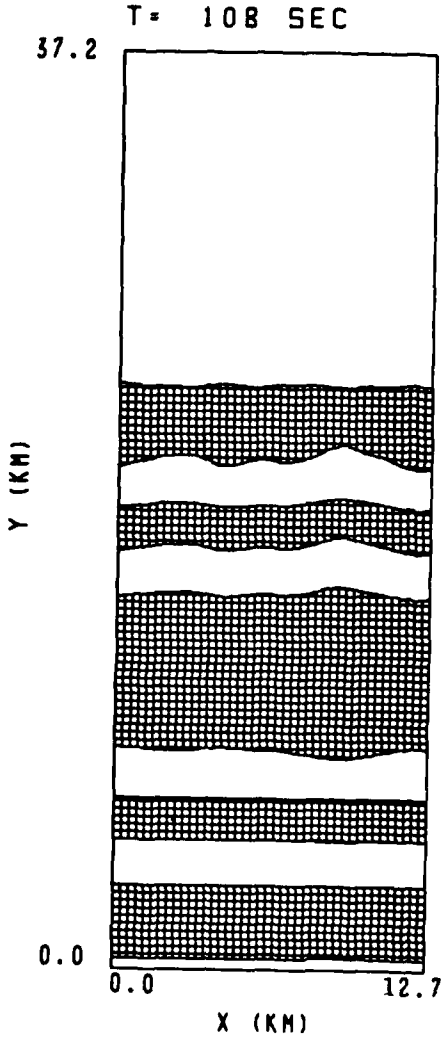


Fig. 17. Same as Fig. 16, but for $t$ = 108 sec. Note slow linear growth on unstable side.

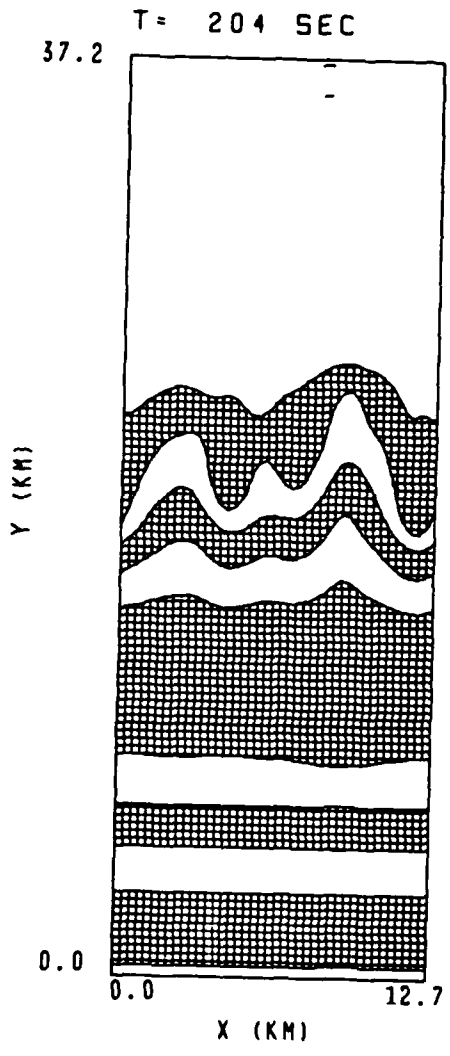


Fig. 18. Same as Fig. 16, but for $t$ = 204 sec. Growth is now much more rapid, and we are entering a highly nonlinear regime.

**Figure 3. Intermediate Contours NRL 3716.**

be the time for the fingering to begin, $4\tau_g$, plus the time for a background finger to break through at the neutral wind speed. For the NRL calculation this is 188 sec.+ 23. 5 km/0. 1 km/sec. = 423 sec.

During the 235 sec. after fingering has begun, the plasma finger moved out at an average speed of half the neutral speed, 50 m/s. We will therefore take the convective displacement of the plasma boundary as $1/2\ V(t - 4\tau_g)$.

What happens after this phase? Another NRL calculation of the same problem was carried out to 720 sec. This is illustrated in the $R_e = \infty$ plot in Figure 4 taken from NRL 3864.[4] The other plots for finite $R_e$ have diffusion added which is too large for the parameter region of interest here.

We find three main fingers with an average convective displacement in agreement with our formula. The boundary at the right is at 50 km and one finger has passed and re-entered on the left (periodic boundary conditions). A second has reached the boundary and a third has not. This calculation[4] solves the same differential equations with the same initial conditions as the other.[3] Slight differences in numerical techniques cause slight differences in the contours which are close enough for our modeling purposes. The interesting phenomenon in this later time picture is the persistence of the original three fingers. Their tips have become small fingers of lesser conductivity but the regions of high conductivity remain intact in the large fingers.

It has been said that after this phase the radial fingers in the nuclear case will be in a uniform neutral wind and will act like Ba clouds. Ba clouds start out spherical, flatten, and finger. Only the tips of these phase 1 fingers act like Ba clouds. We have no numerical calculations or Ba experiments that tell us what happens to the bulk of the highly elongated fingers. We therefore conjecture that after this phase the boundary of the ionization continues to move out at half the neutral wind speed and is made up of two sets of forms. Each of these forms will be described using the four parameter description of a striation whose scintillation effects were described in an earlier paper.[6] The electron density profile is taken as

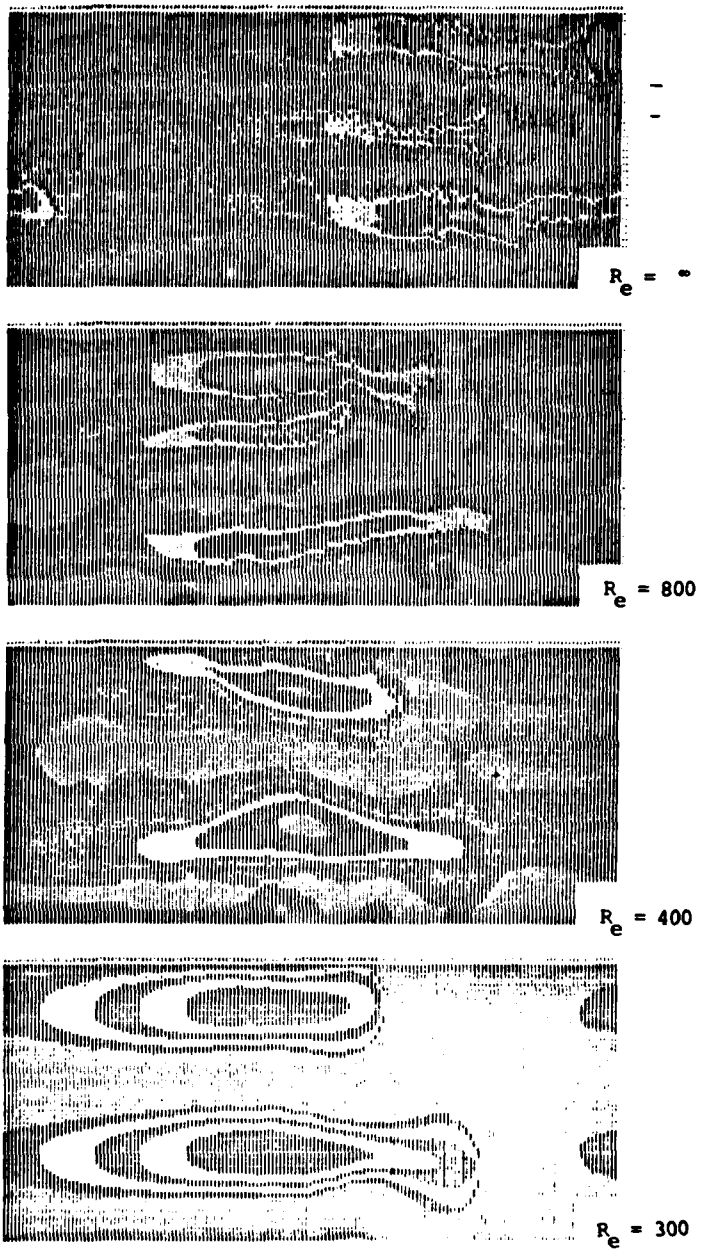


Figure 5

$\Sigma$ contours at T = 720 seconds

**Figure 4. Later Contours NRL 3864.**

$$n_e = n_o\left(1 - \frac{\alpha^2 r^2}{a^2}\right) \quad r \leq a$$

$$= 0 \qquad\qquad r > a$$

where $r^2 = \beta x^2 + y^2/\beta$. Contours of electron density are ellipses with major to minor axes ratio $\beta$. This profile is parabolic from $n_o$ down to $n_1 = n_o(1-\alpha^2)$ where the fall-off is abrupt. The four parameters $n_o$, a, $\alpha$, and $\beta$ describe the striation.

The first set consists of the large striations. The peak electron density, $n_o$, is taken as the peak of the original unstructured ionization. The semi-minor axis is half the finger width

$$\frac{a_L}{\sqrt{\beta_L}} = \frac{\lambda}{4} = \frac{\pi h_{min}}{10} \quad .$$

The specification of $\alpha$ and $\beta$ requires a consistency in preserving the content of $n_e$ and $n_e^2$ in addition to approximating the elongation and profile of the major portion of the content.

The same is true for the second set which represents the secondary fingers. We assign the electron density of the second set the value $n_1 = n_o(1-\alpha^2)$ which makes it dependent on the first set. We assign the value $\alpha = 0$ for the second set for convenience. The initial size of the secondary fingers are half the primary. The semi-minor axis of the second set is then

$$\frac{a_s}{\sqrt{\beta_s}} = \frac{\lambda}{8} = \frac{\pi h_{min}}{20} \quad .$$

The specification of $\alpha$ and the elongation factors $\beta_L$ and $\beta_s$ set the content in each striation. The large striations each have content

$$n_o \pi a_L^2 \left(1 - \alpha^2/2\right)$$

where $a_L^2 = \beta_L(\pi h_{min}/10)^2$. The small striations each have content

$$n_1 \pi a_s^2$$

where $a_s^2 = \beta_s(\pi h_{min}/20)^2$ .

The original content is divided between the two requiring

$$M_L \pi a_L^2\left(1 - \frac{\alpha^2}{2}\right) + M_s\left(1 - \alpha^2\right)\pi a_s^2 = \pi a_o^2$$

where $M_L$ and $M_s$ are the number of large and small striations, $a_o$ is the original Gaussian scale of the unstructured ionization and the factor $(1 - \alpha^2)$ in the second term is $n_1/n_o$. The original unstructured ionization had a squared ionization of $n_o^2 \pi a_o^2/2$ of which division between the two requires $M_L \pi a_L^2(1 - \alpha^2 + \alpha^4/3) + M_s (1 - \alpha^2)^2 \pi a_s^2 = \pi a_o^2/2$ . The solution of the equation is

$$M_L \pi a_L^2 = \frac{\left(2\alpha^2 - 1\right)\pi a_o^2}{\alpha^2\left(1 - \alpha^2/3\right)} \quad ; \quad M_s \pi a_s^2 = \frac{\left(1 - \frac{3}{2}\alpha^2 + \frac{2}{3}\alpha^4\right)\pi a_o^2}{\alpha^2\left(1-\alpha^2/3\right)\left(1-\alpha^2\right)}$$

which requires $\alpha^2 \geq 1/2$. This arises from the constraint of fixing the square of $n_e$ content of a Gaussian by means of parabolic and rod profiles. The model accomplishes the requirements of preserving $n_e$ content and $n_e^2$ content while modeling the large sizes' maintenance of smooth variation and the small sizes existing through pinch-off of large size edge bifurcation. The scintillation effects of the small sizes vanish at $\alpha = 1$.

In order to relate the first set with the scintillation effects described in Reference 6 we redefine $a_L^2(1 - \alpha^2/2) \equiv a^2$ so that the content of a large striation is $n_o \pi a^2$. The results of that study are described in terms of a rather than $a_L$. The original content $n_o \pi a_o^2$ is thus split into $C_L$ and $C_s$ where

$$C_L = n_o M_L \pi a^2 = n_o \pi a_o^2 \frac{(2\alpha^2 - 1)(1 - \alpha^2/2)}{\alpha^2(1 - \alpha^2/3)} \equiv n_o \pi a_o^2 f_L(\alpha)$$

$$C_s = M_s \pi a_s^2 (1 - \alpha^2) n_o = n_o \pi a_o^2 \frac{\left(1 - \frac{3}{2}\alpha^2 + \frac{2}{3}\alpha^4\right)}{\alpha^2 \left(1 - \alpha^2/3\right)} = n_o \pi a_o^2 f_s(\alpha)$$

Once the two contents are established, the further changes in striation morphology are modeled by decreasing a and $a_s$ while keeping $N_L a^2$ and $N_s a_s^2$ constant. In addition further pinch off is modeled by decreasing $\alpha^2$ toward 1/2 thereby increasing $C_s$ at the expense of $C_L$.

# 3. IMPLEMENTATION OF STRUCTURE AND CONVECTION INTO FIREBALL MODEL

The structure model discussed in the last section redistributes the electron content per length along the magnetic field that is predicted by a hydrocode such as MELT. In this section we present an example of that hydrocode output and illustrate the redistribution. We describe the output as a structured RANC fireball.

Since we are using the RANC fireball model as the basic descriptor of the unstructured ionization in general, we will use the MELT output as an interface between the RANC fireball and the structure model since MELT supplies us with an ionization profile whereas RANC does not. The RANC ionization is uniform in the plane perpendicular to the magnetic field.

MRC has kindly supplied us with curves of electron density from a MICE/MELT calculation of a particular high altitude nuclear burst which is representative of yield and burst height to be expected. Figure 5 is an example. We have fit their output at two calculation times, 500 and 1000 sec. by specifying the maximum electron density $n_o(z,t)$ (where z is the distance along the magnetic field) and the total electron content per unit length along z, $C(z,t)$. The content is $n_o \pi a_o^2$ where $a_o^2$ is the product of two characteristic radii from Gaussian fits to the electron density profiles in two directions perpendicular to the magnetic field. An example of the contours of electron density in a plane perpendicular to the magnetic field is shown in Figure 6. The MELT runs show an asymmetry which we ignore in using the symmetric RANC fireball. We do not believe the changes that would be required in the RANC intersection routines to accommodate this asymmetry are warranted.

The RANC fireball model is a truncated ellipsoid described by the parameters:

HF; Height of center (km)

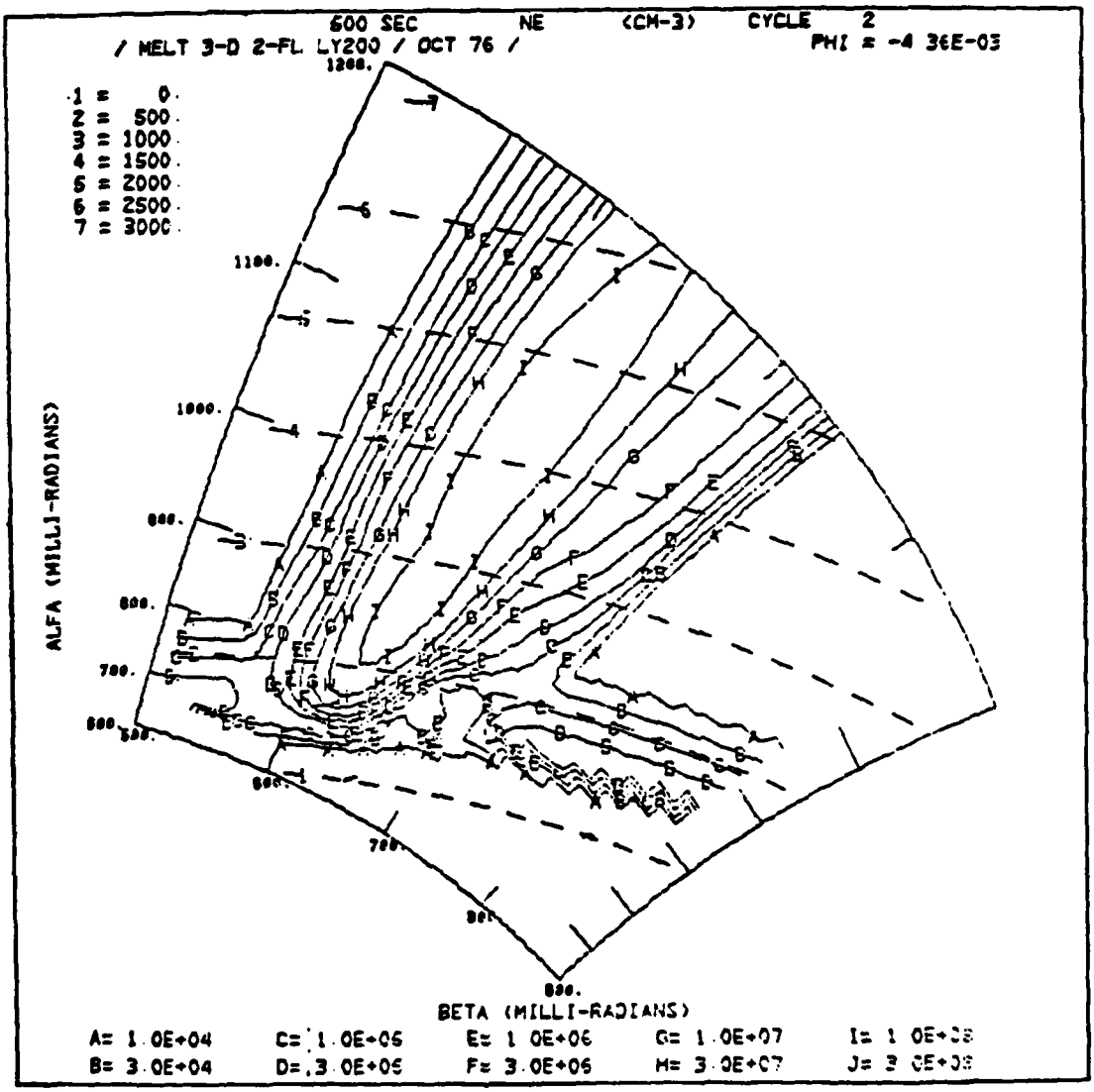


Figure 5. Contours in Plane of Magnetic Field.

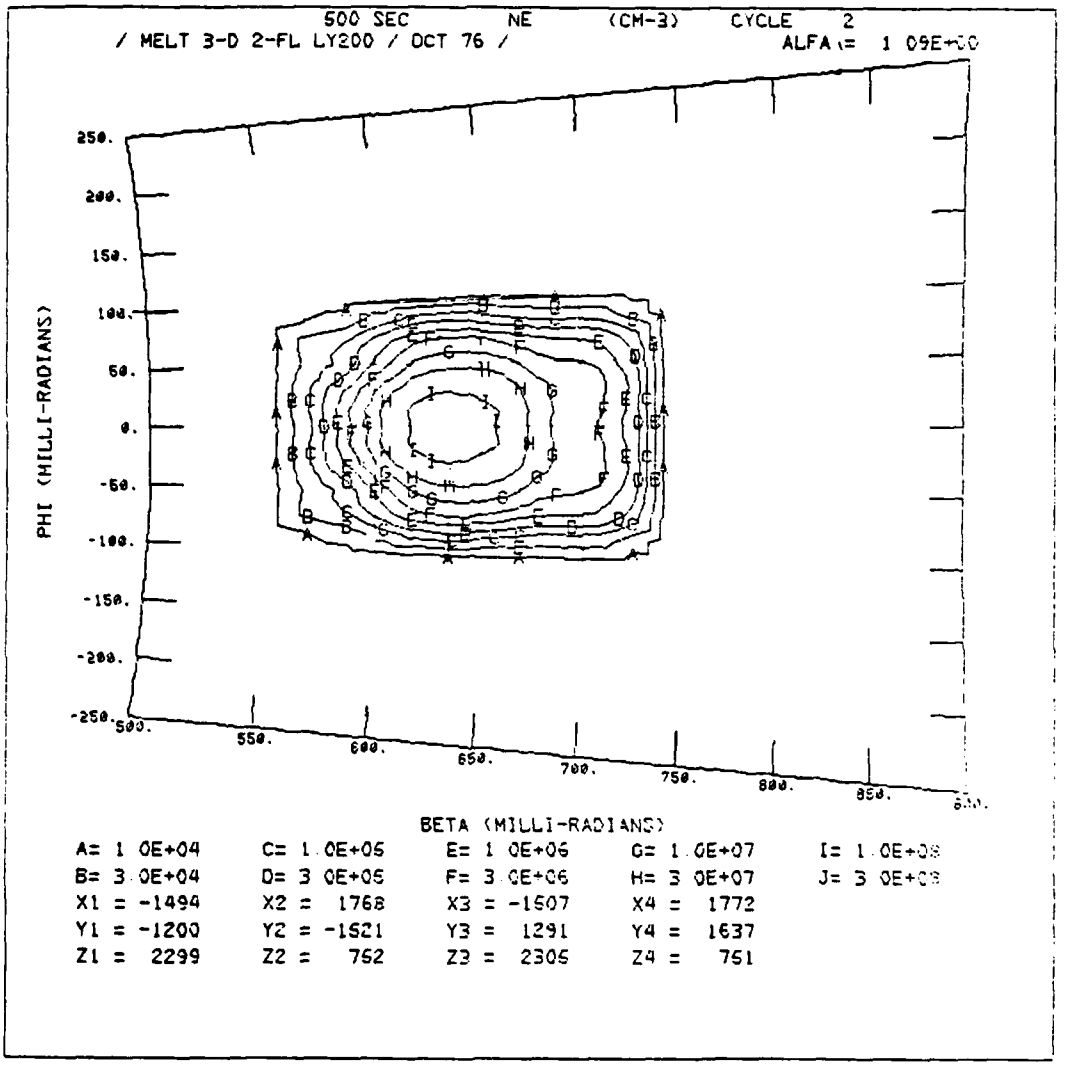


**Figure 6. Contours in Plane Perpendicular to Field.**

RLF; Semi-major axis (along magnetic field) (km)

RTF; Semi-minor axis (km)

TILTF; Cosine of magnetic dip angle

HMINF; Height of fireball bottom (km)

HMAXF; Height of fireball top (km)

Within this ellipsoid RANC prescribes the electron density as a function of height only.

The values of these parameters for the burst and times corresponding to the two MELT runs are:

| Time (sec) | HF | RLF | RTF | TILTF | HMINF | HMAXF |
|---|---|---|---|---|---|---|
| 500 | 1695 | 3199 | 473 | 0.2474 | 335.4 | 4893 |
| 1000 | 1695 | 6063 | 473 | 0.2674 | 220.0 | 7758 |

The resulting shapes are sufficiently close to the MELT contours to use them to contain the ionization content of the MELT runs.

The agreement is good when the RANC ellipsoid is adjusted to lie along the Earth's dipole magnetic field as is currently done in G. E. Tempo's WEPH code[7] and SAI's code NSM.[8] We therefore recommend this adjustment in conjunction with our structure model.

We therefore take the RANC ellipsoid as the boundary of the ionization obtained from MELT. We will be identifying this boundary with the results of the NRL numerical calculation discussed in Section 2 by associating it with the boundary that was above the background and illustrated the fingers. The RANC boundary corresponds to electron density contours two orders of magnitude down from the peak MELT values but higher than the background.

The right way to associate the NRL calculation with the MELT output is through a magnetic field-line integrated Pederson conductivity and a conductivity-weighted field-line integrated neutral wind and other forcing terms obtained from the MELT output. Since we do not have these quantities we cannot accurately evaluate the radius transverse to the field lines where the log-conductivity gradient maximizes. We therefore choose the RANC radius as qualitatively reasonable.

Comparison of a roughly field-line-integrated value of $a_o$ with the RANC radius at 500 sec. shows $a_o \approx RTF/2$. From a previous analysis,[6] we know that a Gaussian profile of conductivity with a maximum value two orders of magnitude over the background has a minimum gradient length $h_{min} = a_o/3$ which is only slightly different for higher maximum to background ratios. We therefore take $h_{min} = RTF/6$.

Typical values of the radial neutral wind speed in hydrocode output run from 100 m/s at a transverse radius of 100 km to 1000 m/s at the fireball edge.[5] In Section 2 we estimated a time of four growth times for the structuring to become evident where the growth time, $\tau_g = h_{min}/V$ where V was uniform. For the nuclear case V varies linearly with radius and is about 750 m/s in the region of maximum initial growth.

In the RANC fireball model, the early radial expansion of the plasma stops at a time, TEQ. At this time after burst when they fix the fireball radius RTF, the plasma is at time zero for the NRL numerical calculation. We therefore set the time for structuring to be observable as

$$\tau_1 = TEQ + 4\,\tau_g = TEQ + \tfrac{2}{3}\,\frac{RTF(km)}{0.75\ km/s}$$

$$= TEQ + \frac{8\,RTF}{9}\ (sec.)\ .$$

For $t < \tau_1$ we consider the fireball to be unstructured.

For $t > \tau_1$, the first phase of structuring proceeds until the background fingers have penetrated to the center of the fireball. In Section 2 this time was determined from a constant velocity. For the nuclear case of radial penetration of background fingers, the velocity has a linear variation with radius which leads to a logarithmic infinite time of penetration. Since the correspondence of the numerical calculation with the nuclear case is best at the plasma edge, we make the analogy of finger displacement at the plasma edge where the plasma fingers (and hence the boundary) convected out an amount $D = \frac{1}{2}V(t - \tau_1)$. The size of the fingers is determined from the scaling law $kh_{min} = 5$ or $k = 30/RTF$ since $h_{min} = RTF/6$. As the plasma fingers move out, the background must move in to preserve the area in the original

circle of radius RTF. The background finger will have the form of a wedge (pie slice) of area (RTF) $\lambda/4 = \pi(RTF)^2/60$ when the background finger reaches the origin. At this time the plasma finger will have an area beyond the original circle corresponding to a half ellipse or $\pi D/2$ $\lambda/4$ which will equal the pie slice when $D = 2\,RTF/\pi$ at the time

$$\tau_2 = \tau_1 + \frac{2D}{V} = \tau_1 + \frac{4\,RTF}{\pi V}$$

where $V \approx 1$ km/s.

At the end of this time the boundary of the striated ionization will be at $RTF + 2\,RFT/\pi$. The structure is described by the parameters mentioned in Section 2. The parameter $\alpha$ distributes the content C between the two sets of sizes, determines the profile of the large sizes, and the relative electron density, $n/n_o$, of the small sizes. The large sizes have maximum electron density $n_o(z)$. We shall begin at $t = \tau_1$ with $\alpha = 1$ and end at $\tau_2$ with $n_1/n_o = (1-\alpha^2) = 1/20$ which is the ratio of conductivity where the gradient length h is smallest to the maximum conductivity. At the same time we will be turning on the structure with a coefficient that linearly rises from zero at $\tau_1$ to unity at $\tau_2$ to represent the structuring.

For $\alpha^2 \approx 1$ we have from Section 2, $C_L \approx \frac{3}{4} n_o \pi a_o^2$ and $C_s \approx \frac{1}{4} n_o \pi a_o^2$.

For the initial number of large fingers we use the criterion $k = 30/RTF$ which signifies the number of fingers, $M_L$, to be 30 since that is the number of wavelengths around the circumference of the ionization. Therefore equating the formulas for content, $30\, n_o \pi a_L^2/2 = \frac{3}{4} n_o \pi a_o^2$ or $a_L^2 = a_o^2/20 = (RTF)^2/80$. From Section 2 $a_L^2 = \beta_L (\pi h_{min}/10)^2 = \beta_L (\pi RTF/60)^2$. Therefore $\beta_L = (60/\pi)^2/80 \simeq 4.6$.

Since the small set represents the bifurcation of the tips of the large fingers, their number and elongation are not constant. Also, since we are commited to conserving the $n_e$ and $n_e^2$ content of a Gaussian profile using non-Gaussian profiles we suffer the consequence that the initial content of the small fingers be one quarter the total which is not true. Their initial scintillation effects however are $\propto n_e^2$ and start from zero. We shall set the initial size of

the small fingers so that their width is half that of the large fingers so

$$a_s^2 = \beta_s\left(\frac{\pi h_{min}}{20}\right)^2 = \beta_s\left(\frac{\pi RTF}{120}\right)^2 .$$

We expect $\beta_s \approx \beta_L = 4.6$ so we will let their number be determined from the content formulas. Choosing the large size as $a_L = RTF/9$ says the initial small size is $a_s = RTF/18$.

For $t > \tau_2$, we expect the striations to continue their radial convection but further structuring, if any, will not be apparent until after the last time of the numerical calculation shown in Figure 4 of Section 2. Because of the high elongation ($\beta$) and high conductivity ratio to background and lower slip velocity (neutral speed-cloud speed) we expect further structuring to take a relatively long time. It would seem reasonable that the smaller fingers continue to grow at the expense of the large fingers. The larger fingers' higher conductivity will flow into the small fingers.

By allowing $\alpha$ to approach $\frac{1}{2}$, we will deplete the large fingers. We expect further bifurcation to occur in the small fingers. The typical way this occurs need not result in a much smaller finger width since the fingers can widen from the filling before bifurcating. Thus as $\alpha^2 \to \frac{1}{2}$, the electron density in the small fingers and their number increase and their size decreases by only half. We have no numerical calculations or experimental data that are late enough to fix the time for the end of this phase when $\alpha^2 = \frac{1}{2}$. We shall take this time as the time for the high density ($n = n_o/2$) to overtake the boundary. The high density is taken as $\frac{1}{2}$ the original peak since this is the final value of density in the small finger when $\alpha^2 = \frac{1}{2}$. By the analysis in Section 2, the high density portion should travel at the local neutral wind speed while the boundary will continue to travel at half of the local neutral wind speed. At $t = \tau_2$, the boundary is at $RB = RTF(1 + 2/\pi)$ and the high density is at $RH = 0.6\ RTF$. We take the neutral wind speed as $V = MIN\ (r/RTF,\ 1)$ km/s which is the speed of the high conductivity portion. The high density position a time $t$ later is

$$RH = RTF + t - RTF\ \ln(5/3) = 0.49\ RTF + t$$

where the last term in the middle is the time to reach r = RTF.

$$RB = RTF\left(1 + \frac{2}{\pi}\right) + \frac{t}{2} \text{ km}$$

$$= 1.637\ RTF + 0.5\ t\ .$$

We find RH = RB at t = 2.29 RTF after $\tau_2$. We therefore define

$$\tau_3 = \tau_2 + 2.29\ RTF$$

when we are left with only the small set of striations described as elliptical "waterbags" ($\beta = 4.6$, $\alpha = 0$) of ionization $n_1 = n_o/2$ and size $a_s = RTF/36$.

If they were truly waterbags they would not structure further if they were in a uniform neutral wind according to the analysis of Section 2. We know that any departure from these idealized conditions cause them to structure further until they reach some stable size whose value has not yet been determined for the nuclear case. At this stage the striations are similar to barium clouds. In a previous analysis[6] we invoked a bifurcation time which depended on the structure parameters and conductivity ratio $\chi$. Since this time was proportional to the striation size, each bifurcation time was progressively shorter. From barium experiments there appeared to be a minimum size where bifurcation ceased. The reason for this has not yet been discovered so scaling to the nuclear case cannot be done at this time. Assuming therefore the nuclear case will be similar to the barium case we chose $a_m = 200$ m. We implement this by the formula from reference 6 which says the time to reach size $a$ from an initial size $a'$ is

$$t(a, a') = \tau_o\left(a' - a + \frac{16\ a_m^2}{a - a_m} - \frac{16\ a_m^2}{a' - a_m}\right)$$

where

$$\tau_o = \frac{4.3\sqrt{\beta}}{V_n}\left(1 + \frac{1}{\chi}\right)\left(1 + \beta + \beta\chi\right)$$

let

$$a_o = a' - \frac{t(a, a')}{\tau_o}$$

and

$$a_1 = \frac{16\, a_m^2}{a' - a_m}$$

then

$$a = \frac{1}{2}\left\{a_o + a_m - a_1 + \sqrt{\left(a_o - a_m\right)^2 - 2a_1\left(a_o + a_m - 2a'\right) + a_1^2}\right\}$$

We choose the parameters $\chi = 4$, $\beta = 4.6$, $V_n = 0.5$ km/s and get $\tau_o = 553$ s/km.

So for time t after $\tau_3$ when $a_o = a' - (t - \tau_3)/553$, $a_m = 0.2$, and $a_1 = 0.64/(a' - 0.2)$ where $a' = RTF/36$ we use the above formula for $a_s$.

To summarize:

Given RTF (km) and TEQ (sec.) from the RANC code;

Define $\tau_1 = TEQ + 8/9\ RTF$ (sec.),

$\tau_2 = \tau_1 + 4/\pi\ RTF$ (sec.),

and $\tau_3 = \tau_2 + 2.29\ RTF$ (sec.) .

Define a structure factor S as a multiplier for the scintillation effects to be introduced later. The time independent parameters of structure are $\beta_L = \beta_s = 4.6$, $a_L = RTF/9$, $a_m = 0.2$ km. The time dependent structure parameters are $\alpha$ and $a_s$. The boundary of the striations is at RB.

For $t \leq \tau_1$

$$S = 0, \quad RB = RTF \ .$$

For $\tau_1 < t \leq \tau_2$

$$a_s = \frac{RTF}{18} \ , \quad S = \frac{t - \tau_1}{\tau_2 - \tau_1}$$

$$\alpha^2 = 1 - \frac{S}{20} \ , \quad RB = RTF + \frac{(t - \tau_1)}{2} \ .$$

For $\tau_2 < t \leq \tau_3$

$$a_s = \frac{RTF}{18}\left[1 - \frac{(t - \tau_2)}{2(\tau_3 - \tau_2)}\right] \ , \quad S = 1 \ ,$$

$$\alpha^2 = 1 - \frac{1}{20} - \frac{9}{20}\,\frac{(t - \tau_2)}{(\tau_3 - \tau_2)} \ , \quad RB = RTF + \frac{(t - \tau_1)}{2}$$

For $t > \tau_3$

$$S = 1 \ , \quad \alpha^2 = \frac{1}{2} \ ,$$

$$RB = RTF + \frac{(t - \tau_1)}{2} \ .$$

$$a_s = \frac{1}{2}\left\{a_o - a_m - a_1 + \sqrt{(a_o - a_m)^2 - 2a_1(a_o + a_m - 2a') + a_1^2}\right\}$$

where

$$a_o = a' - \frac{(t - \tau_3)}{553} \ ,$$

$$a_1 = \frac{16\, a_m^2}{a' - a_m} \ , \quad a' = \frac{RTF}{36} \ .$$

The final portion of the fireball model is the stipulation of the unstructured content $C = n_o \pi a_o^2 = n_o \pi/4\,(RTF)^2$ and the peak ionization $n_o$. The RANC model outputs an ionization, ENE, which is a decreasing function of distance from the bottom along the magnetic field but is uniform within the area $\pi R^2$ where R is the transverse radius of the RANC ellipsoid with semi-minor axis RTF. At that point

$$ENE\ \pi(RTF)^2 = n_o \pi(RTF)^2/4$$

or $$n_o = 4\ ENE\ .$$

We chose $a_o$ = RTF/2 as an approximation for a field line integrated average. By using the 2-D NRL run we are saying the mixing and convection of the plasma occur by rearrangement of the contents of flux tubes. This means that while the plasma boundary is fingering where R = RTF, nothing is happening up the field lines where there is only background at R = RTF. This means the higher regions should be retarded in their structuring compared to the lower regions. We cannot model this effect now. Since we must work with the RANC elliptic fireball we simply make the substitution of RB for RTF and let the upper part of the ellipse expand accordingly. We maintain the parameters of structure throughout the fireball. For any point along the field line, the RANC-predicted unstructured content is

$$ENE\ \pi(RTF)^2 \left(1 - \frac{z^2}{(RLF)^2}\right).$$

We will take $n_o$ = 4 ENE throughout thereby implying that the Gaussian scale also *decreases with z in the same manner. The implication of this choice is that the* number of striations per unit area are independent of z.

## 4. SCINTILLATION EFFECTS

The scintillation effects of the structure model were determined in Reference 6 for a single size. The scintillation effects for the two sets are obtained by adding their $\varphi_{eff}^2$ defined in that reference extended to the case where the ray path is not perpendicular to the magnetic field but is at an angle $\theta_B$. For the set of large sizes

$$\varphi_L^2 = \frac{\varphi_{oL}^2}{1 + \frac{1}{\left(1 - \alpha^2\right)^2 \frac{3\pi\epsilon}{4} + \alpha^4\left(1 - \alpha^2/2\right)\frac{315}{16}\epsilon^2\left(\frac{3}{2} - \ell n\epsilon\right)}}$$

where

$$\varphi_{oL}^2 = \frac{16\, a^3 \Gamma_L \left(r_e \lambda n_o\right)^2}{3 \sin\theta_B} N_L P$$

where

$$a^2 = a_L^2\left(1 - \frac{\alpha^2}{2}\right) \quad , \quad \epsilon = \frac{\Gamma_L^2 \lambda d}{8\pi a^2} \quad ,$$

$\Gamma$ is a scale factor caused by striation ellipticity which will be described later.

$r_e = 2.818 \cdot 10^{-13}$ cm.

$\lambda$ = signal wavelength.

$N_L$ = number of striations per unit area perpendicular to the magnetic field.

$P$ = ray path length through the striations.

$d = d_1 d_2/(d_1 + d_2)$ and $d_1$ and $d_2$ are the two distances between the two terminals and the striations.

The striations lie within an area $\pi(RB)^2$ in the plane perpendicular to the magnetic field. Therefore

$$N_L = \frac{M_L}{\pi(RB)^2} = \frac{C_L}{n_o \pi^2 a^2 (RB)^2} = \frac{a_o^2 f_L(\alpha)}{\pi a^2 (RB)^2} = \frac{(RTF)^2}{(RB)^2} \frac{f_L(\alpha)}{4\pi a^2} .$$

For the set of small sizes

$$\varphi_S^2 = \frac{\dfrac{16 a_S^3 \Gamma_S \left(r_e \lambda n_o\right)^2 \left(1 - \alpha^2\right)^2 N_S P}{3 \sin \theta_B}}{1 + \dfrac{32 a_S^2}{3 \Gamma_S^2 \lambda d}} = \frac{\varphi_{oS}^2}{1 + \dfrac{32 a_S^2}{3 \Gamma_S^2 \lambda d}}$$

where

$$N_S = \frac{f_S(\alpha)}{4\pi a_S^2 \left(1 - \alpha^2\right)} \frac{(RTF)^2}{(RB)^2}$$

The total

$$\varphi_{eff}^2 = \varphi_L^2 + \varphi_S^2 .$$

The scale factor

$$\Gamma = \sqrt{\frac{\beta}{1 + (\beta^2 - 1) \sin^2 \theta_i}}$$

which is a scale factor derived in Reference 6 where $\theta_i$ is the angle between the long axis of the elliptic striation and the projection of the LOS in the plane perpendicular to the magnetic field.

As a typical LOS penetrates the striated region there will be a range of values of $\theta_i$ and hence $\Gamma$ will be a weighted average which will be near $\sqrt{\beta}$ for a LOS crossing near the center of the striations and near $1/\sqrt{\beta}$ for a LOS passing near the endge of the striated region. As explained in Reference 6, this occurs because the striations have their long axes pointing radially from the center of the striated region in the plane perpendicular to the magnetic field. This is modeled by choosing $\theta_i = \cos^{-1} (P \sin \theta_B / 2\, RB)$.

The correlation length of the scintillations

$$\ell \approx \frac{a}{2\Gamma\varphi_o\sqrt{1 - \alpha^2/2}}$$

according to the single size analysis of Reference 6. The extension of the analysis to two sizes defines $\ell$ by the equation

$$\frac{1}{\ell^2} = 4\left[\frac{\Gamma_L^2\varphi_{oL}^2(1 - \alpha^2/2)}{a^2} + \frac{\Gamma_S^2\varphi_{oS}^2}{a_S^2}\right]$$

The quantities $\varphi_{eff}^2$ and $\ell$ are the primary descriptors of the scintillation effects. Scintillation in the received signal intensity is measured by the scintillation index $S_4$ defined by

$$S_4^2 \equiv \overline{I^2} - 1$$

where I is the signal intensity at the receiver normalized to intensity in the absence of structure in the ionization. The average intensity $\overline{I} = 1$ by conservation of energy. From the analysis of Reference 6,

$$S_4^2 \approx 1 - e^{-2\varphi_{eff}^2}$$

meaning intensity scintillation is negligible for $\varphi_{eff}^2 \ll 1$ and essentially Rayleigh for $\varphi_{eff}^2 \geq 1$. When Rayleigh, $\ell$ is the autocorrelation length of $I - \overline{I}$. In general $\ell$ is the length such that $\overline{E(x)E^*(x + \ell)} = 1/\sqrt{e} = 0.606$ where $E = \sqrt{I}e^{i\varphi}$ where the phase $\varphi$ is produced by the structure and $x$ is distance perpendicular to the plane defined by the LOS and the magnetic field. Therefore in the absence of intensity scintillation, $\ell$ has meaning for phase scintillation

$$\overline{e^{i[\varphi(x) - \varphi(x + \ell)]}} = e^{-\frac{1}{2}\overline{[\varphi(x) - \varphi(x + \ell)]^2}} = e^{-\frac{1}{2}}$$

$$\text{or} \quad \overline{[\varphi(x) - \varphi(x + \ell)]^2} = 1 \ .$$

The translation of correlation length to correlation time requires the x component of velocity of the LOS with respect to the striations. This is sufficient if the striations' motion is negligible. We have the striations moving across the magnetic field at speeds around 500 m/s. If the LOS passes near center, very little striation motion is in the x direction. If the LOS passes near the edge of the striated region the striation motion is mainly in the x direction. We therefore take $V_x = 0.5$ km/s $\sin \theta_i$ where $\theta_i$ was used in the definition of $\Gamma$ and choose the sign according to whether the LOS is moving radially outward or inward. That is, the correlation time

$$\tau = \frac{\ell}{|V_{xLOS} \pm 0.5 \sin \theta_i|}$$

This formula erroneously allows $\tau$ to become infinite. We know the differential movement of the striations will cause $\tau$ to always be finite. The determination of $\tau$ for differentially moving striations is a task for future work.

## 5. IMPLEMENTATION INTO AN EXISTING CODE

In any existing systems code that uses RANC phenomenology, there is a routine that describes the fireball. In RANC, the routine is called PHENOM. In that routine the type of high-altitude fireball that our structure model is pertinent to is magnetically contained so that after a defined magnetic containment time TEQ, the semi-minor axis of the ellipsoidal fireball, RTF, is held constant at the magnetic containment radius RM. In PHENOM, this type of fireball is designated by setting the flag KINDF = 2. We save the radius RM for use as RTF in our structure formulas and change the boundary by setting RTF = RB according to the formulas of Section 3 thereby expanding the fireball to account for the striation convection.

There is also a routine that computes the attenuation and scintillation effects. In RANC, the routine is called ABSORB. It calls a routine, XFBT, that determines the intersection of the line of sight between two antennas and the fireball. It then steps along the total path length, PL, of the intersection adding up the absorption in dB and the mean-square scintillating phase, $\varphi_o^2$, according to its own structure formula. These two quantities are proportional to the square of the local electron density, ENE, which it obtains from the subroutine ENEFB. At this point we change ENE to correspond to the mean square electron density of our expanded fireball. Therefore

$$\overline{n_e} = \mathrm{ENE}\left(\frac{\mathrm{RM}}{\mathrm{RTF}}\right)^2$$

but

$$\overline{n_e^2} = \frac{n_o \overline{n_e}}{2} = 2\ \mathrm{ENE}\ \overline{n_e}$$

since $n_o = 4$ ENE.

For the absorption formula we replace ENE by $\sqrt{2}$ ENE(RM/RTF).

For scintillation effects we need $n_o^2 = 16(ENE)^2$ at each step to obtain

$$\varphi_{oL}^2 = \frac{64\ Sa}{3\pi}\ \Gamma_L f_L \left(\frac{r_e \lambda RM}{RTF}\right)^2 \sum_{steps} \frac{(ENE)^2(\Delta P)_{step}}{\sin\theta_B}$$

and

$$\varphi_{oS}^2 = \frac{a_s \Gamma_s f_s\ (1 - \alpha^2)}{a \Gamma_L f_L}\ \varphi_{oL}^2 \ .$$

The determination of $\Gamma_s = \Gamma_L$ described in Section 3 requires information unobtainable from the RANC intersection routine, XFBT, without altering the routine. We therefore approximate the average angle between the LOS and the striation axis as

$$\theta_i = \cos^{-1}\left(\sum_{steps} \frac{\Delta P \sin\theta_B}{2\ RTF}\right)$$

for the formula

$$\Gamma_s = \Gamma_L = \sqrt{\frac{\beta}{1 + (\beta^2 - 1)\sin^2\theta_i}} \ .$$

The formulas for a, $a_s$, $\beta$, $f_s$, $f_L$, $\alpha$, and S given in Section 3 are implemented to evaluate and output $\varphi_{eff}$ and $\ell$ from the formulas in Section 4 .

The RANC code outputs the velocity of the LOS perpendicular to the magnetic field. What is needed is the component of that velocity in the x direction and the position of the LOS intersection in the fireball in order to compute correlation time. Without this information we suggest bounding the correlation time using V = 500 m/s added to and subtracted from the given LOS velocity with a minimum value of 50 m/s for the denominator in the formula $\tau = \ell / |V_{LOS} \pm 0.5|$ .

## 6. LIST OF REFERENCES


1. Jordano, R., et al., "Revised Nuclear Phenomenology and Radar Propagation Models for RANC IV," General Electric Tempo (unpublished).

2. Sachs, D. L., "Propagation Effects of Steep Striations," DNA 4170T, Nov November 1976.

3. Zalesak, S. T., "Fully Multidimensional Flux-Corrected Transport," NRL Memorandum Report 3716, May 1978.

4. McDonald, B. E., S. L. Ossakow, S. T. Zalesak, and N. J. Zabusky, "A Fluid Model for Estimating Minimum Scale Sizes in Ionospheric Plasma Cloud Striations," NRL Memorandum Report 3864, October 30, 1978.

5. Kilb, R. W., and W. W. White, personal communication, December 1978.

6. Sachs, D. L., L. M. Linson, and D. C. Baxter, "Characteristics of Striation Structure and Effects on Scintillation," DNA4612F, May 1978.

7. Knapp, W. S., "WEPH VI: A Fortran Code for the Calculation of Ionization and Electromagnetic Propapgation Effects Due to Nuclear Detonation," General Electric Tempo (unpublished).

8. Smith, C. A., personal communication, November 1978.

# DISTRIBUTION LIST

DEPARTMENT OF DEFENSE

Assistant to the Secretary of Defense
Atomic Energy
ATTN: Executive Assistant

Defense Nuclear Agency
ATTN: DDST
ATTN: STVL
3 cy ATTN: RAAE
4 cy ATTN: TITL

Defense Technical Information Center
12 cy ATTN: DD

Field Command
Defense Nuclear Agency
ATTN: FCPR

Field Command
Defense Nuclear Agency
Livermore Division
ATTN: FCPRL

Undersecretary of Defense for Rsch. & Engrg.
ATTN: Strategic & Space Systems (OS)

DEPARTMENT OF THE ARMY

Harry Diamond Laboratories
Department of the Army
ATTN: DELHD-N-P

DEPARTMENT OF THE NAVY

Naval Research Laboratory
ATTN: Code 6780, S. Ossakow

DEPARTMENT OF THE NAVY (Continued)

Naval Surface Weapons Center
ATTN: Code F31

DEPARTMENT OF THE AIR FORCE

Air Force Weapons Laboratory, AFSC
ATTN: SUL
ATTN: DYC

DEPARTMENT OF DEFENSE CONTRACTORS

ESL, Inc.
ATTN: J. Marshall

General Electric Company-TEMPO
ATTN: DASIAC

General Research Corp.
ATTN: J. Ise, Jr.

Mission Research Corp.
ATTN: R. Hendrick
ATTN: R. Bogusch

R & D Associates
ATTN: C. MacDonald

Science Applications, Inc.
ATTN: D. Sachs
ATTN: L. Linson

SRI International
ATTN: W. Chesnut
ATTN: C. Rino